ARTICLE

Unraveling Nonradiative Effects and Reaction Mechanism of Aza-Paternò-Büchi Reaction Catalyzed by a Cu(I) Complex

Xin-Xin Liu[a], Jia-Jia Ma[a], Ling-Ya Peng[b*], Qiu Fang[a*], Ganglong Cui[a]

a. Key Laboratory of Theoretical and Computational Photochemistry, Ministry of Education, College of Chemistry, Beijing Normal University, Beijing 100875, China
b. Shaanxi Key Laboratory of New Concept Sensors and Molecular Materials, Key Laboratory of Applied Surface and Colloids Chemistry, Ministry of Education, School of Chemistry and Chemical Engineering, Shaanxi Normal University, Xi'an 710119, China

(Dated: Received on May 28, 2025; Accepted on June 25, 2025)

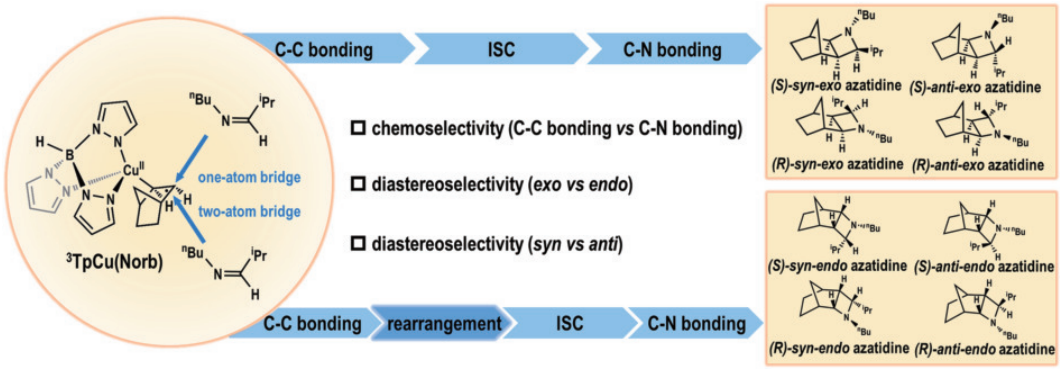

The azetidine heterocyclic framework, a four-membered nitrogen-containing ring system, is prevalent in natural product derivatives and pharmacological compounds. As one of the powerful tools for generating azetidine, photocycloaddition catalyzed by Cu complex has achieved great success. However, the mechanism at the atomic level remains elusive. Herein, by combining the density functional theory (DFT) and time-dependent DFT (TD-DFT) methods, the reaction mechanism and the physical origin of diastereomeric selectivity are explored comprehensively. Our calculations reveal that tris(pyrazolyl)borate Cu (TpCu) initially coordinates with norbornene (Norb) to generate TpCu(Norb) complex. Upon photoexcitation, TpCu(Norb) can eventually populate the triplet state, in which the C=C double bond is activated. The initial C–C bonding reaction occurs in the triplet state, followed by an intersystem crossing process to the ground state, where the C–N bond forms. Depending on the spatial orientation of the approaching imine, either from one-atom bridge (-CH_2- group) or from two-atom bridge (-CH_2-CH_2- group), products with *exo*- and *endo*-diastereomers can be generated. Notably, a structural rearrangement is required to form the *endo*-products. Both *syn*- and *anti*-diastereomers are observed as products in the transformation due to the relative orientations of imine and Norb. The present work not only unlocks the detailed reaction mechanism but also provides valuable insights into the construction of azetidine.

Key words: Photocycloaddition, Transition metal complexes, Density functional theory, Reaction mechanism, Nonadiabatic process

I. INTRODUCTION

Cyclobutane derivatives such as oxetane, cyclobutene, azetidine, and thietane, represent pivotal

* Authors to whom correspondence should be addressed.
E-mail: lingya.peng@snnu.edu.cn, fangqiu917@bnu.edu.cn

scaffolds in natural products, drug discovery, and organic synthesis [1–5]. To construct cyclobutane derivatives, photocycloaddition reactions have been widely employed, which involve the direct excitation of substrates such as alkynes, carbonyls or imines and followed by another alkene interception [1, 6–16]. The premier photocycloaddition refers to the Paternò-Büchi reaction, enabling the reaction between carbonyl and alkene forming oxetanes [17–19]. Analogous to the Paternò-Büchi reaction, aza Paternò-Büchi reaction between imines and alkenes has emerged as a powerful tool for forming azetidine [20–23]. However, upon excitation, a facile photoisomerization of the C=N bond may occur, leading to a reduction in reaction efficiency [20–22]. Furthermore, the limited number of photoactive substrates also impede both the practicability and generality of this scope [9]. Thus, the development of new diagram to access cyclobutane derivatives remains highly desirable.

Photocatalysis has made a new entrance to the conventional [2+2] photocycloaddition reaction, which expands the scope of substrates significantly [2, 7, 8, 24–33]. Distinguished by the reaction diagram, photocatalysis relies on the excitation of the photosensitizer succeeded by the efficient electron/energy transfer to one of the substrates, which then reacts with the other and concludes the reaction cycle [34]. The photosensitizers of Ru and Ir complexes have attained remarkable success in this field [29, 35]. Yoon *et al.* have reported a class of photocycloaddition reactions with enantioselectivity, which are triggered by the excitation of $[Ru(bpy)_3]^{2+}$ [36, 37]. Becker *et al.* have investigated the synthesis of azetidines from oximes and alkynes, where triplet-state oxime formed by the energy transfer from an Ir-photosensitizer was recognized as a key intermediate [10]. Brown *et al.* have developed the Ir complex photosensitized cycloaddition of styrenyl dihaloboranes and allylamines, forming cyclobutylboranes with stereoselectivity and regioselectivity [38–40]. And a temporary coordination between dihaloboranes and amines was observed, which plays an important role in the reaction [41]. However, the energy dissipation of the electron or energy transfer cannot be ignored in this pattern, calling for a new model.

Transition metal complexes have built a novel blueprint for photocatalysis, where a single complex can play dual roles, *i.e.*, absorbing light and catalyzing the reactions [42, 43]. Notably, substrate coordination to Cu centers enables *in situ* formation of photoactive Cu complexes which are capable of direct light excitation. Salomon, Kochi, Jayasekara, and their co-workers have discovered the dimerization reactions of norbornenes and cyclohexenes, which pave new avenues for photocatalysis [44–46]. The Cu complexes of metal and olefins are formed initially and then excited via metal-to-ligand charge transfer (MLCT) processes. Flores *et al.* have extended this model to the Paternò-Büchi and aza Paternò-Büchi reactions catalyzed by tris(pyrazolyl)borate Cu (TpCu). Upon coordination of norbornene to the TpCu, the resulting complex undergoes light-induced MLCT activation, facilitating the formation of oxetane and azetidine, respectively [23, 32].

Although substantial experimental achievements have been accomplished, a comprehensive mechanistic understanding is still lacking, demanding detailed theoretical studies to unravel the underlying reaction mechanism. Our group has previously studied the Paternò-Büchi reaction of norbornene and ketones [47], as well as the photodimerization reactions of norbornenes and cyclohexenes [48]. Based on our research, different photophysical processes are observed, resulting in the population of the ^{3}MLCT and ligand-centered state (^{3}LC), respectively. And the nonradiative transitions play critical roles in either photophysical processes or reaction pathways. However, the mechanism of the aza Paternò-Büchi reaction catalyzed by TpCu is still elusive. And the origin of the observed diastereoselectivity (95:5 *exo*:*endo*) remains unclear.

In the present work, a comprehensive study on the reaction trajectories is conducted to clarify the mechanism of *N*-butyl-2-methylpropan-1-imine and norbornene by utilizing the combination of DFT and TD-DFT calculations. The catalytic reactions, as well as the origin of the diastereoselectivity, have been systematically elucidated. Our work not only establishes a fundamental mechanistic understanding of the aza Paternò-Büchi reaction but also provides new insights for the rational design of the photocycloaddition reaction.

II. COMPUTATIONAL METHODS

All DFT calculations were conducted using Gaussian16 [49]. The B3LYP functional was employed with a mixed basis set (referred to as BS-I), incorporating the SDD pseudopotential and basis sets for Cu atom, while the 6-31G** basis sets were utilized for the C, H, B, and

DOI: 10.1063/1674-0068/cjcp2505073

N atoms [50–56]. To account for the weak dispersion interactions, the Grimme dispersion scheme (D3) was implemented, and the solvent effects of diethyl ether were implicitly considered by the polarizable continuum model (PCM) [57, 58]. Structural optimizations were followed by frequency analysis at the same theoretical level to verify the nature of minima (with no imaginary frequency) and transition states (only having one imaginary frequency). The intrinsic reaction coordinate (IRC) calculations were applied to confirm transition states connecting optimized minima (including reactants, intermediates, and products) [59]. For more accurate energy evaluations, single-point energies were performed at the (U)B3LYP-D3/PCM level using an extended mixed basis set (BS-II). For the C, H, B, and N atoms, all electron 6-311++G** basis sets were adopted [60, 61]. For the Cu atom, SDD pseudopotential and SDD basis sets were adopted. Additionally, the minimum-energy crossing points (MECPs) between T_1 and S_0 states were determined with sobMECP [62]. Energy decomposition analysis scheme based on the generalized Kohn-Sham (GKS-EDA) calculations at the (U)B3LYP-D3/BS-II/PCM level was carried out using GAMESS (2021, R2) [63–65]. The total binding energy can be decomposed into the electrostatic, correlation-dispersion, polarization, exchange-repulsion, and desolvation energy terms, respectively.

The calculations of spin-orbit coupling (SOC) matrix elements and oscillator strengths between different electronic states were performed using the LR-TDDFT method within the same B3LYP functional the Tamm-Dancoff approximation (TDA-B3LYP) [66, 67]. In this section, the RI-SOMF(1X) method adopting scalar relativistic all-electron calculations with Douglass-Kroll-Hess Hamiltonian of second order (DKH2), was used [68–72]. All-electron SARC-DKH-TZVP basis set was used for the Cu atom, while DKH-def2-TZVP basis sets were used for the C, H, B, and N atoms [73–77]. The solvent effects of diethyl ether were considered using the conductor-like PCM method. To accelerate the computation of two electron integrals, both the resolution of identity approximation for the Coulomb part (RIJ) and the chain of spheres algorithm for the exchange part (COSX) with the corresponding auxiliary basis sets and the grid settings, were employed [78, 79]. All these SOC matrix elements and oscillator strengths calculations were performed using ORCA 6.0.1 [80]. $\langle S_a|\widehat{H}_{SO}|T_b\rangle$ is the effective SOC between singlet and triplet states calculated as follows:

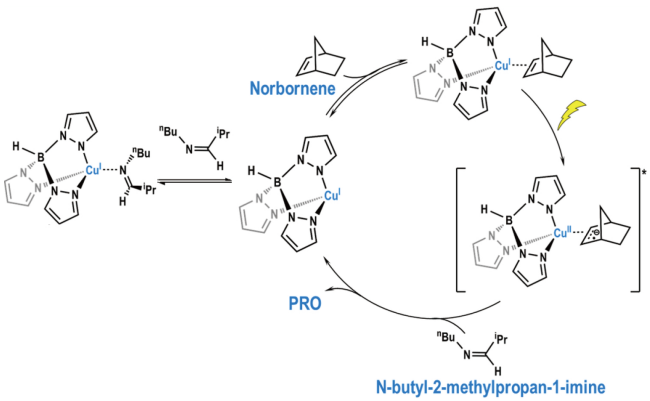

FIG. 1 Experimentally proposed mechanism for the Cu-catalyzed [2+2] photocycloaddition of norbornene and *N*-butyl-2-methylpropan-1-imine.

$$\langle S_a|\widehat{H}_{SO}|T_b\rangle = \sqrt{\left(\langle S_a|\widehat{H}_x^{SO}|T_b\rangle\right)^2+\left(\langle S_a|\widehat{H}_y^{SO}|T_b\rangle\right)^2+\left(\langle S_a|\widehat{H}_z^{SO}|T_b\rangle\right)^2}$$

where the $|S_a\rangle$ and $|T_b\rangle$ are singlet and triplet electronic wavefunctions; $\widehat{H}_x^{SO}$, $\widehat{H}_y^{SO}$, and $\widehat{H}_z^{SO}$ are spin-orbit operators of x, y, and z components.

III. RESULTS AND DISCUSSION

A. The formation of *exo*-azetidine

Experimental studies have elucidated the photocycloaddition mechanism in the reaction between *N*-butyl-2-methylpropan-1-imine (Imine) and norbornene (Norb) to form azetidines (see FIG. 1) [23]. The proposed catalytic cycle involves dynamic coordination of TpCu with Norb or Imine, selective Norb binding to generate TpCu(Norb), photoinduced Cu-alkene charge transfer, and the cycloaddition reaction with Imine.

According to the ^{1}H NMR spectroscopy of TpCu, Norb, and Imine, the ligand exchange can happen between TpCu(Norb) and TpCu(Imine) [23]. However, the isolation of the TpCu(Imine) was unsuccessful, implying the reversibility of this process. To elucidate the interactions between TpCu and Norb, the energy decomposition analysis is employed (see FIG. 2). The electrostatic interactions become the main driving force for these processes with –75.7 kcal/mol. However, the exchange-repulsion interactions put significant obstacles of 102.7 kcal/mol. This can be rationalized by examining the ground state structures. In TpCu(Norb), the Cu is coordinated to both C1 and C2 atoms (Cu–C1: 2.065 Å and Cu–C2: 2.064 Å). The pronounced steric effects in TpCu(Norb) result in an increase in the ex-

DOI: 10.1063/1674-0068/cjcp2505073

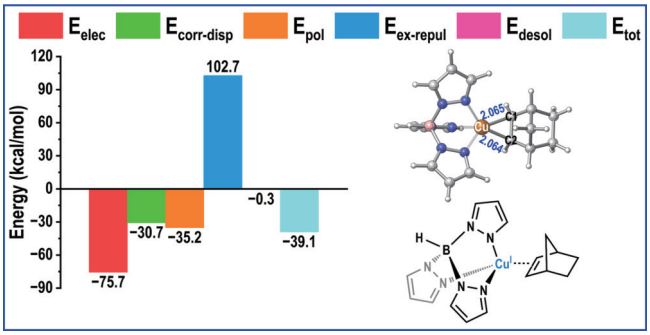

FIG. 2 Energy decomposition analysis for TpCu(Norb).

change-repulsion energy.

Upon excitation, the ^{3}MLCT state of TpCu(Norb) is populated eventually, which is the precursor state of the following reaction [47]. Furthermore, the cycloaddition reactions are systematically investigated. It is noteworthy that the MLCT process effectively activates the C1=C2 bond, and the repopulation of electrons generates Cu(II) and C1 radical. The Imine can undergo a nucleophilic attack by the C1 atom of ^{3}TpCu(Norb). The diastereoselectivity governed by norbornene attack via either one-atom (the -CH_2- group) or two-atom bridges (the -CH_2-CH_2- group), as well as the Imine orientation during bond formation, remains unresolved (see FIG. 3). And there are two bonding processes leading to the azetidines formation: C–C bonding and C–N bonding. The chemoselectivity of C1–C3 versus C1–N prior formation also plays a critical role in determining the enantiomeric outcome.

Starting from the ^{3}MLCT state of TpCu(Norb), the cycloaddition pathway is initiated when attacking the Imine from the one-atom bridge. The complex ^{3}1a, consisting of ^{3}TpCu(Norb) and Imine, is formed through a process involving partial electron transfer to the Imine moiety (TpCu(Norb): 1.63, Imine: 0.37). This observation suggests the activation of the Imine, as evidenced by elongation of the C=N bond to 1.300 Å (cf. 1.271 Å in free Imine), indicative of a reduced bond order. In addition, a key structural feature of ^{3}1a is that the H3 atom in C=N of the Imine adopts a *syn*-configuration relative to the hydrogen atom at the ring junction moiety of Norb, and this spatial arrangement is conserved throughout the reaction trajectory. Then, C1–C3 bonding is facile to happen with a negligible free-energy barrier of 3.8 kcal/mol and releases 5.2 kcal/mol during formation from ^{3}1a to ^{3}2a, accompanied by the intramolecular electron transfer from the C1 atom to the N atom (^{3}1a, C1: 0.74 and N: 0.19; ^{3}2a, C1: 0.04 and N: 0.96). From ^{3}2a, a rearrangement reaction involving concurrent Cu–N bond formation (Cu–N: 1.855 Å) and Cu–C2 bond cleavage (Cu–C2: 4.496 Å) occurs, which corresponds to a 2.1 kcal/mol free-energy barrier and is exothermic by 9.7 kcal/mol at the B3LYP-D3/BS-II level, leading to a more stable intermediate ^{3}3a. During this transformation, the electron reorganization is also monitored from Cu and N atoms to the C2 atom (^{3}3a, Cu: 0.29, C2: 0.99, N: 0.62), which shifts to the sp^2 hybridization of C2 (107.9°, 124.3°, 123.4°) at ^{3}3a from sp^3 hybridization (104.3°, 112.1°, 111.8°) at ^{3}2a. The subsequent C2–N bond formation in the triplet state encounters a substantial activation barrier ($\Delta G^{\ddagger}$ = 58.1 kcal/mol) and exhibits a significant energy difference (ΔG = 37.6 kcal/mol) from ^{3}3a.

Considering the unfavorable thermodynamics and high free-energy barrier from ^{3}3a, the second C–N bond formation should occur exclusively in the ground state. Consequently, the intersystem crossing to the ground state is examined. Notably, two competitive channels can hop to the ground state (FIG. 4). One is directly via the minimum energy crossing point (MECP) from ^{3}2a, the structure of MECP_2a is similar to ^{3}2a, leading to a close energy between them with an energy gap of only 0.1 kcal/mol. The other involves advancing to ^{3}3a first, which requires an additional energy of 2.1 kcal/mol and then proceeds through an ISC process to the ground state. The former is kinetically more favorable, and the ground state is effectively populated with an ISC rate of $k_{ISC} = 1.2\times10^{10}$ s^{-1} (see FIG. S1 in Supplementary materials, SM), yielding the strained five-membered ring species ^{1}2a. This ISC process is also coupled with electron transfer from the Cu center to the N atom, inducing a change in the Cu oxidation state from +II to +III. From the intermediate ^{1}2a, subsequent C–N bond formation happens upon overcoming a moderate energy barrier of 4.7 kcal/mol and releasing 17.0 kcal/mol to generate the stable azetidine product, (*S*)-*syn*-*exo*-azetidine (^{1}4a). In addition, the reaction pathway in the ground state is systematically investigated. The free energy barrier is 57.0 kcal/mol from ^{1}TpCu(Norb) for the first C–C bonding, which quantitatively demonstrates that photoexcitation is the requisite to initiate the reaction process (see FIG. S2 in SM).

Analogously, when the Imine adopts an *anti*-configuration relative to the Norb moiety, the reaction proceeds through a mechanistically similar pathway, ultimately yielding the (*R*)-*anti*-*exo*-azetidine isomer ^{1}4b

DOI: 10.1063/1674-0068/cjcp2505073

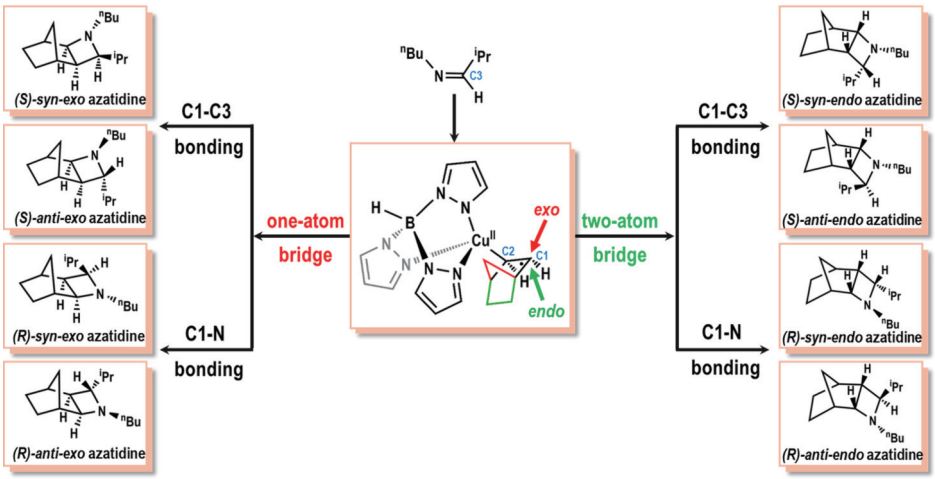

FIG. 3 Proposed reaction pathways from ^{3}TpCu(Norb) and *N*-butyl-2-methylpropan-1-imine (Imine) and the resulting products with different chemoselectivity and diastereoselectivity.

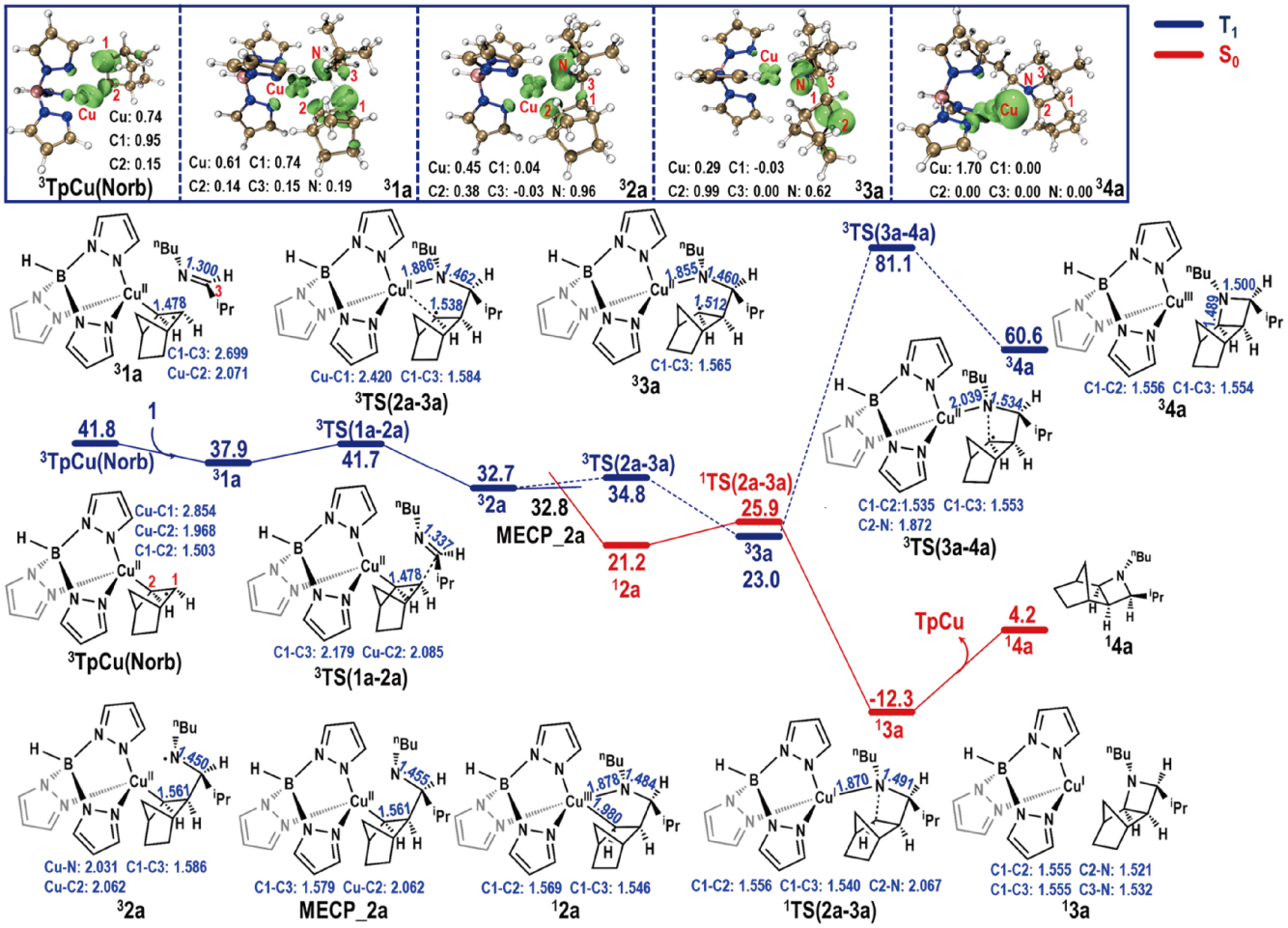

FIG. 4 Free-energy profile (in kcal/mol), calculated at B3LYP-D3/PCM level, of [2+2] cycloaddition reactions for (*S*)-*syn*-*exo*-azetidine (^{1}4a), in which the C1–C3 bond is formed preferentially. Also shown are selected bond lengths (in Å) and spin populations. See text for discussion.

(see FIG. S3 in SM). The energy discrepancy between ^{1}4a and ^{1}4b reflects the diastereoselectivity observed experimentally, which is attributed to the lower free-energy barrier and the more favorable steric interactions along the *syn*-pathway.

In addition, the preferential formation of the C–N

DOI: 10.1063/1674-0068/cjcp2505073

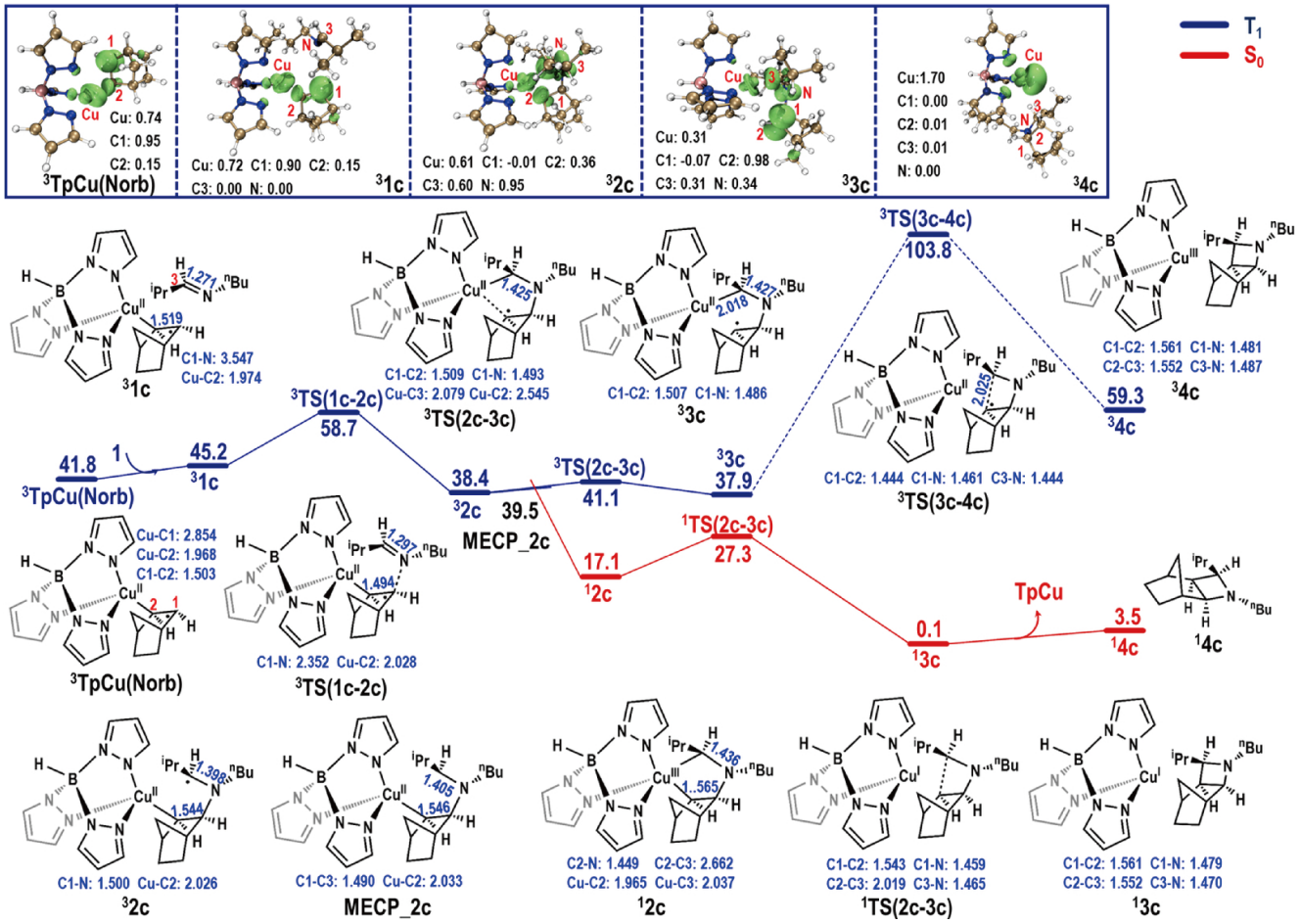

FIG. 5 Free-energy profile (in kcal/mol), calculated at B3LYP-D3/PCM level, of [2+2] cycloaddition reactions for the (*R*)-*syn*-*exo*-azetidine (^{1}4c), in which the C1–N bond is formed preferentially. Also shown are selected bond lengths (in Å) and spin populations. See text for discussion.

bond is thoroughly evaluated (see FIG. 5). Unexpectedly, a higher energy barrier is identified for the C–N bond formation pathway, calculated to be 13.5 kcal/mol from ^{3}1c. This process is recognized as the rate-limiting step, with a small exothermic driving force (ΔG=–6.8 kcal/mol). The rearrangement reaction from ^{3}2c to ^{3}3c also readily happens after releasing 0.5 kcal/mol. The modest driving force stems from the single electron repopulation between the C2 and C3 atoms, wherein Cu retains coordination to the carbon atoms. This behavior contrasts with the intermediate ^{3}3a, where the transition from Cu–C to Cu–N bonding introduces enhanced electrostatic interactions, stabilizing the intermediate. Similarly, ISC is accessible either directly via MECP_2c with rate $k_{ISC}=3.4\times10^5$ s^{-1} (see FIG. S6 in SM), or via a ^{3}3c-mediated process from ^{3}3c to ^{1}2c. Then, from ^{1}2c, the subsequent C–C bonding is detected. And (*R*)-*syn*-*exo*-azetidine ^{1}4c is mainly formed, corresponding to the enantiomer of the previously described ^{1}4a.

Differently, for the formation of (*S*)-*anti*-*exo*-azetidine ^{1}4d, the first C–N bonding corresponds to a reduced free-energy barrier of 9.3 kcal/mol, which is primarily attributed to the small steric hindrance of ^{3}TS(1d-2d). After the system is effectively populated in the S_0 state, the Cu–C3 is formed with a bond length of 2.040 Å in ^{1}2d, where the C–C bonding takes place after overcoming a 13.0 kcal/mol free-energy barrier and releasing 17.4 kcal/mol at the B3LYP-D3/BS-II level (see FIG. S8 in SM).

Noteworthy, the free-energy barrier associated with C–N bonding exceeds that of the C–C formation pathway by 9.7 and 4.8 kcal/mol for the *syn*- and *anti*-configurations, respectively. This kinetic preference emerges from fundamental aspects of the nucleophilic attack mechanism. Specifically, in comparison with the N atom, the C3 center exhibits substantially greater electrophilicity, as evidenced by their Mulliken charges

DOI: 10.1063/1674-0068/cjcp2505073

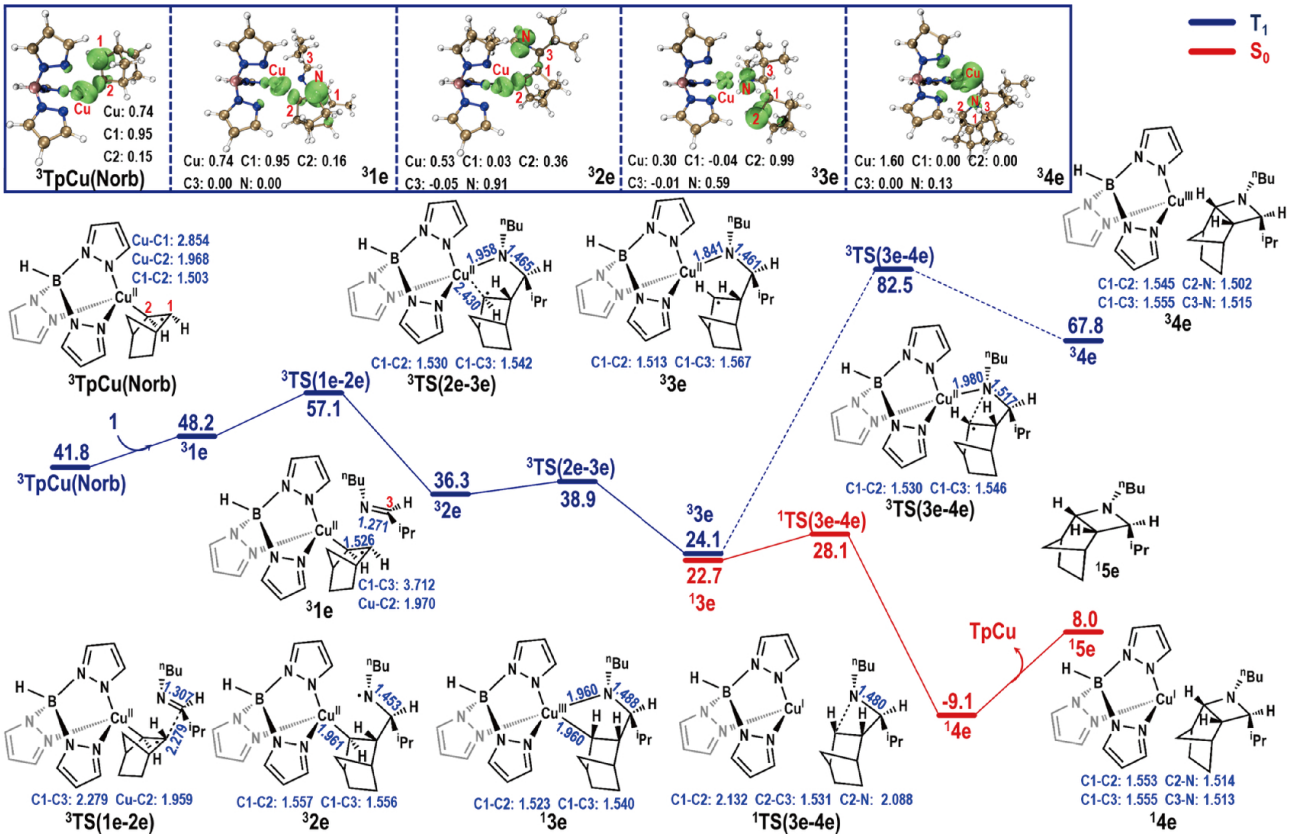

FIG. 6 Free-energy profile (in kcal/mol), calculated at B3LYP-D3/PCM level, of [2+2] cycloaddition reactions for the (*S*)-*anti-endo*-azetidine (^{1}4e), in which the C1–C3 bond is formed preferentially. Also shown are selected bond lengths (in Å) and spin populations. See text for discussion.

of 0.181 |e| (N: –0.332 |e|) of ^{1}3c (see Table S6 in SM). Consequently, the C–C preferential bond formation becomes the more favorable pathway. According to our calculations, the 4a with (*S*)-configuration is mainly formed with prior selectivity than the enantiomer 4c with (*R*)-configuration. However, the experiments declared no detectable enantioselectivity. This discrepancy can be attributed to the quasi-symmetrical structure of TpCu(Norb). Upon photoexcitation, either the Cu–C1 bond (as currently studied) or the Cu–C2 bond may cleave. When the latter species coordinates with the Imine, it would correspondingly generate enantiomers of (*R*)-*syn-exo*-azetidine analogous to (*S*)-*syn-exo*-azetidine. Thus, the reaction pathways are indistinguishable in terms of both thermodynamic stability and kinetic feasibility for the identical steric constraints [47].

B. The formation of *endo*-azetidine

While the ^{3}TpCu(Norb) attacks the Imine via the two-atom bridge, the first C–C bond formation occurs upon surmounting an 8.9 kcal/mol energy barrier, forming ^{3}2e, which refers to the rate-limiting process (FIG. 6). Unlike the previous pathway, where the intermediates, such as ^{3}2a, adopt a *cis*-configuration of the hydrogen at the ring junction region, ^{3}2e exists in a *trans*-conformation. Although we initially considered a direct ISC from ^{3}2e to the ground state (analogous to the *exo*-azetidines formation pathway), this route is disfavored due to the increased ring strain that would require a subsequent ground-state isomerization. Instead, ^{3}2e preferentially undergoes isomerization by overcoming a small barrier of 2.6 kcal/mol to form ^{3}3e, which is an exothermic process releasing 12.2 kcal/mol. The transition state ^{3}TS(2e-3e) involves characteristic Cu–C bond cleavage and Cu–N bond formation similar to the previous steps, coupled with a conformational inversion of the hydrogen of Norb from *trans* to *cis*, ultimately yielding the more stable intermediate ^{3}3e. The ISC process from ^{3}3e becomes more favorable with a small energy gap of 1.4 kcal/mol, producing ^{1}3e with the five-membered ring. From ^{1}3e, a C–N bonding process takes place with liberating 14.7 kcal/mol, forming the (*S*)-*anti-endo*-product. Similarly, the (*R*)-*syn-endo*-

DOI: 10.1063/1674-0068/cjcp2505073

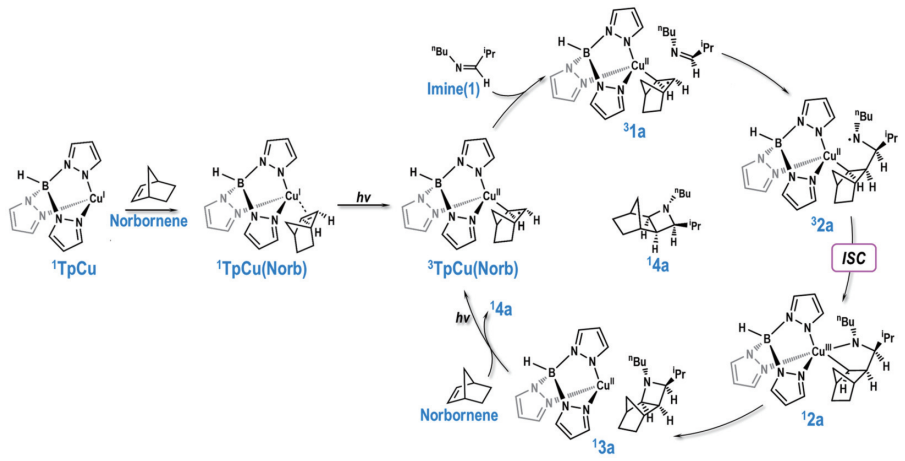

FIG. 7 Proposed photocatalytic reaction mechanism for the (*S*)-*syn*-*exo*-azetidine. See text for discussion.

product can also be formed, with the free-energy barrier of the rate-limiting process being 13.6 kcal/mol (see FIG. S13 in SM). Moreover, for the pathway favoring C–N bond formation, less favorable kinetics are observed, leading to preferential C–C bond formation, consistent with the *exo*-product generation pathway (see FIGs. S15 and S18 in SM).

C. Correlation of calculations and experiments

Photoinduced TpCu-catalyzed cycloaddition can efficiently construct azetidines, but the atomistic mechanism remains unclear. Our calculations not only reveal the detailed mechanism but also provide some novel insights (see FIG. 7). The active species of TpCu(Norb) is first formed. Upon excitation, the ^{3}MLCT state is eventually populated to initiate the cycloaddition. From ^{3}TpCu(Norb), the chemoselectivity is explored to determine whether the C–C or C–N bonding happens first. And the C–N bonding processes correspond to unfavorable kinetics or thermodynamics. Thus, the C–C bonding is preferred to take place from ^{3}TpCu(Norb) for the stronger nucleophilicity of the C atom in the Imine. Moreover, the diastereoselectivity of the reaction relies on the approach trajectory of the Imine, *i.e.*, one-atom bridge (-CH_2- group) or two-atom bridge (-CH_2-CH_2- group), leading to the formation of *exo*- and *endo*-products, respectively. The different potential energy surfaces are observed. In the *exo*-product formation pathways, three steps are required: C–C bonding, ISC, and C–N bonding. Nevertheless, the rearrangement is the prerequisite for the *endo*-scaffold formation, which alleviates the ring strain induced by the *trans*-configuration of the hydrogen atom and generates a more stable intermediate. This process also influences the hybridization mode of the C1 atom from sp^3 to sp^2. In other words, the synergistic interplay between electronic and steric effects modulates this rearrangement reaction. Due to the higher free-energy barrier ($\Delta G^{\ddagger} = 8.9$ kcal/mol) and unfavorable thermodynamics, the *endo*-product remains a minor component. Furthermore, altering the relative orientation of the imine toward TpCu(Norb) can also govern stereoselectivity. When the hydrogen of the Imine and the hydrogen at the ring junction of the Norb moiety are in the same direction, the configuration is designated as *syn*; conversely, it is *anti*. Our computational studies reveal that in the case of the *exo*-product, the formation of the *syn*-azetidine is favored, while the *endo*-product preferentially yields the *anti*-azetidine.

Although our calculations exclusively predict the formation of the (*S*)-enantiomer, no enantioselectivity was observed experimentally. This discrepancy arises from symmetry breaking during photoexcitation of TpCu(Norb). When the system accesses an alternative excited-state conformation involving Cu–C1 bond cleavage, the reaction pathway becomes energetically comparable but preferentially yields the (*R*)-enantiomer, thereby canceling out overall enantioselectivity. In a word, the reaction proceeds through C–C bond formation, followed by intersystem crossing to the ground state, where subsequent C–N coupling selectively generates the *exo*-product. In contrast, the *endo*-product forming pathway involves C–C bonding, excited-state structural rearrangement, ISC process, and subsequent C–N coupling.

DOI: 10.1063/1674-0068/cjcp2505073

IV. CONCLUSION

In this work, a mechanistic investigation of the Cu-catalyzed photocycloaddition between norbornene and *N*-butyl-2-methylpropan-1-imine was carried out by using TD-DFT and DFT methods. Initially, photoexcitation prompts the TpCu(Norb) populated in the triplet state, along with the activation of the C=C double bond, thereby triggering the succeeding cycloaddition reaction to generate *exo*- or *endo*-azetidine via different attack directions. In terms of the kinetics, the C–C bond forms preferentially in the triplet state. It is worth noting that to yield *endo*-azetidine, the rearrangement process is necessary. Finally, the system undergoes an effective ISC process to the ground state, and then the C–N bond is formed to yield the products. This work provides deeper insights into the reaction characteristics and mechanism, which should be useful for understanding and further promoting the photoinduced Cu-catalyzed cycloaddition reaction.

Supplementary materials: Computational methods of rate calculations, MECP structures, free-energy profiles, free-energy along reaction profiles, Mulliken charges of intermediate in reaction profiles and Cartesian coordinates of all optimized structures.

V. ACKNOWLEDGMENTS

This work was supported by the National Key Research and Development Program of China (No.2021YFA1500703), the National Natural Science Foundation of China (No.22233001 and No.22288201), the Fundamental Research Funds for the Central Universities, and Innovation Program for Quantum Science and Technology (No. 2021ZD0303305).

[1] K. Malarney, S. Kc, and V. Schmidt, Org. Biomol. Chem. **19**, 8425 (2021).
[2] S. Poplata, A. Tröster, Y. Zou, and T. Bach, Chem. Rev. **116**, 9748 (2016).
[3] M. D'Auria and R. Racioppi, Molecules **18**, 11384 (2013).
[4] H. Mughal and M. Szostak, Org. Biomol. Chem. **19**, 3274 (2021).
[5] J. Xu, Beilstein J. Org. Chem. **16**, 1357 (2020).
[6] Q. B. Zhang, F. Li, B. Pan, L. Yu, and X. G. Yue, Chem. Eur. J. **30**, e202401501 (2024).
[7] S. Y. Hou, B. C. Yan, H. D. Sun, and P. T. Puno, Nat. Prod. Bioprospect. **14**, 37 (2024).
[8] M. Golfmann, L. Glagow, A. Giakoumidakis, C. Golz, and J. Walker, Chem. Eur. J. **29**, e202202373 (2023).
[9] P. Franceschi, S. Cuadros, G. Goti, and L. Dell'Amico, Angew. Chem. Int. Ed. **62**, e202217210 (2023).
[10] M. Becker, E. Wearing, and C. Schindler, Nat. Chem. **12**, 898 (2020).
[11] B. Xu, X. Shi, X. Liu, and H. Cao, Molecules **27**, 359 (2022).
[12] Y. Liu, Y. Chen, S. Ma, X. Liu, X. Zhang, J. Zou, and L. Pan, Fuel **318**, 12369 (2022).
[13] W. Z. Z. Michalska, N. R. R. Halcovitch, and S. C. C. Coote, Chem. Commun. **59**, 784 (2023).
[14] D. Qi, J. Bai, H. Zhang, B. Li, Z. Song, N. Ma, L. Guo, L. Song, and W. Xia, Green Chem. **24**, 5046 (2022).
[15] M. Zhu, X. Zhang, C. Zheng, and S. You, Acc. Chem. Res. **55**, 2510 (2022).
[16] E. Kumarasamy, S. Kandappa, R. Raghunathan, S. Jockusch, and J. Sivaguru, Angew. Chem. Int. Ed. **56**, 7056 (2017).
[17] M. D'Auria, Photochem. Photobiol. Sci. **18**, 2297 (2019).
[18] D. Zhang, C. Wu, H. Zhou, Y. Ma, and Y. Zhu, Asian J. Org. Chem. **11**, e202200561 (2022).
[19] E. Kumarasamy, R. Raghunathan, S. K. Kandappa, A. Sreenithya, S. Jockusch, R. B. Sunoj, and J. Sivaguru, J. Am. Chem. Soc. **139**, 655 (2017).
[20] S. Kandappa, L. Valloli, S. Ahuja, J. Parthiban, and J. Sivaguru, Chem. Soc. Rev. **50**, 1617 (2021).
[21] A. Richardson, M. Becker, and C. Schindler, Chem. Sci. **11**, 7553 (2020).
[22] E. R. Wearing, Y. C. Yeh, G. G. Terrones, S. G. Parikh, I. Kevlishvili, H. J. Kulik, and C. S. Schindler, Science **384**, 1468 (2024).
[23] D. Flores, M. Neville, and V. Schmidt, Nat. Commun. **13**, 2764 (2022).
[24] C. Prier, D. Rankic, and D. MacMillan, Chem. Rev. **113**, 5322 (2013).
[25] J. Parthiban, D. Garg, S. Ahuja, S. Jockusch, A. Ugrinov, and J. Sivaguru, ACS Catal. **14**, 8794 (2024).
[26] C. Feng, Y. Liu, Z. Xiang, X. Cheng, S. Wei, X. Liu, Q. Deng, Q. Fu, and Z. Zhang, Chem. Eur. J. **30**, e202403881 (2024).
[27] R. Takagi and T. Tanimoto, Org. Biomol. Chem. **20**, 3940 (2022).
[28] D. Blackmun, S. Chamness, and C. Schindler, Org. Lett. **24**, 3053 (2022).
[29] F. M. Hoermann, C. Kerzig, T. S. Chung, A. Bauer, O. S. Wenger, and T. Bach, Angew. Chem. Int. Ed. **59**, 9659 (2020).
[30] S. Ha, Y. Lee, Y. Kwak, A. Mishra, E. Yu, B. Ryou, and C. M. Park, Nat. Commun. **11**, 2509 (2020).
[31] S. Ahuja, S. Jockusch, A. Ugrinov, and J. Sivaguru, Eur. J. Org. Chem. **2020**, 1478 (2020).
[32] D. Flores and V. Schmidt, J. Am. Chem. Soc. **141**, 8741 (2019).
[33] V. Mojr, G. Pitrová, K. Straková, D. Prukala, S. Brazevic, E. Svobodová, I. Hoskovcová, G. Burdzinski,

DOI: 10.1063/1674-0068/cjcp2505073

T. Slanina, M. Sikorski, and R. Cibulka, ChemCatChem **10**, 849 (2018).
[34] K. Cheung, S. Sarkar, and V. Gevorgyan, Chem. Rev. **122**, 1543 (2022).
[35] Z. C. Girvin, L. F. Cotter, H. Yoon, S. J. Chapman, J. M. Mayer, T. P. Yoon, and S. J. Miller, J. Am. Chem. Soc. **144**, 20109 (2022).
[36] E. M. Sherbrook, H. Jung, D. Cho, M. H. Baik, and T. P. Yoon, Chem. Sci. **11**, 856 (2020).
[37] Z. D. Miller, B. J. Lee, and T. P. Yoon, Angew. Chem. Int. Ed. **56**, 11891 (2017).
[38] S. Adak, P. S. Hazra, C. B. Fox, and M. K. Brown, Angew. Chem. Int. Ed. **64**, e202416215 (2025).
[39] J. M. Posz, N. Sharma, P. A. Royalty, Y. Liu, C. Salome, T. C. Fessard, and M. K. Brown, J. Am. Chem. Soc. **146**, 10142 (2024).
[40] Y. Liu, D. Ni, B. G. Stevenson, V. Tripathy, S. E. Braley, K. Raghavachari, J. R. Swierk, and M. K. Brown, Angew. Chem. Int. Ed. **61**, e202200725 (2022).
[41] Y. Liu, D. Ni, and M. K. Brown, J. Am. Chem. Soc. **144**, 18790 (2022).
[42] K. L. Skubi, T. R. Blum, and T. P. Yoon, Chem. Rev. **116**, 10035 (2016).
[43] R. Jin, X. Y. Guo, L. Y. Peng, X. Y. Liu, W. H. Fang, and G. Cui, Chin. J. Chem. Phys. **37**, 87 (2024).
[44] R. G. Salomon and J. K. Kochi, J. Am. Chem. Soc. **96**, 1137 (1974).
[45] R. G. Salomon, K. Folting, W. E. Streib, and J. K. Kochi, J. Am. Chem. Soc. **96**, 1145 (1974).
[46] G. Jayasekara, C. Antolini, M. Smith, D. Jacoby, J. Escolastico, N. Girard, B. Young, and D. Hayes, J. Am. Chem. Soc. **143**, 19356 (2021).
[47] L. Y. Peng, R. Jin, S. R. Zhang, X. Y. Liu, W. H. Fang, and G. Cui, J. Org. Chem. **89**, 11334 (2024).
[48] X. X. Liu, J. J. Ma, G. Li, L. Y. Peng, Q. Fang, W. H. Fang, and G. Cui, Phys. Chem. Chem. Phys. **27**, 13588 (2025).
[49] M. J. Frisch, G. W. Trucks, H. B. Schlegel, G. E. Scuseria, M. A. Robb, J. R. Cheeseman, G. Scalmani, V. Barone, G. A. Petersson, H. Nakatsuji, X. Li, M. Caricato, A. V. Marenich, J. Bloino, B. G. Janesko, R. Gomperts, B. Mennucci, H. P. Hratchian, J. V. Ortiz, A. F. Izmaylov, J. L. Sonnenberg, D. Williams-Young, F. Ding, F. Lipparini, F. Egidi, J. Goings, B. Peng, A. Petrone, T. Henderson, D. Ranasinghe, V. G. Zakrzewski, J. Gao, N. Rega, G. Zheng, W. Liang, M. Hada, M. Ehara, K. Toyota, R. Fukuda, J. Hasegawa, M. Ishida, T. Nakajima, Y. Honda, O. Kitao, H. Nakai, T. Vreven, K. Throssell, J. A. Montgomery Jr., J. E. Peralta, F. Ogliaro, M. J. Bearpark, J. J. Heyd, E. N. Brothers, K. N. Kudin, V. N. Staroverov, T. A. Keith, R. Kobayashi, J. Normand, K. Raghavachari, A. P. Rendell, J. C. Burant, S. S. Iyengar, J. Tomasi, M. Cossi, J. M. Millam, M. Klene, C. Adamo, R. Cammi, J. W. Ochterski, R. L. Martin, K. Morokuma, O. Farkas, J. B. Foresman, and D. J. Fox, *Gaussian 16, Rev. A. 03*, Wallingford, CT: Gaussian Inc., (2016).
[50] A. D. Becke, J. Chem. Phys. **98**, 1372 (1993).
[51] A. D. Becke, Phys. Rev. A **38**, 3098 (1988).
[52] S. H. Vosko, L. Wilk, and M. Nusair, Can. J. Phys. **58**, 1200 (1980).
[53] C. T. Lee, W. T. Yang, and R. G. Parr, Phys. Rev. B **37**, 785 (1988).
[54] P. C. Harihara and J. A. Pople, Theor. Chim. Acta. **28**, 213 (1973).
[55] R. Ditchfield, W. J. Hehre, and J. A. Pople, J. Chem. Phys. **54**, 724 (1971).
[56] P. J. Hay and W. R. Wadt, J. Chem. Phys. **82**, 299 (1985).
[57] S. Grimme, J. Antony, S. Ehrlich, and H. Krieg, J. Chem. Phys. **132**, 154104 (2010).
[58] V. Barone and M. Cossi, J. Phys. Chem. A **102**, 1995 (1998).
[59] K. Fukui, Acc. Chem. Res. **14**, 363 (1981).
[60] T. Clark, J. Chandrasekhar, G. W. Spitznagel, and P. V. Schleyer, J. Comput. Chem. **4**, 294 (1983).
[61] R. Krishnan, J. S. Binkley, R. Seeger, and J. A. Pople, J. Chem. Phys. **72**, 650 (1980).
[62] T. Lu, *sobMECP program*, http://sobereva.com/286, accessed May, (2025).
[63] Z. Tang, Y. Song, S. Zhang, W. Wang, Y. Xu, D. Wu, W. Wu, and P. Su, J. Comput. Chem. **42**, 2341 (2021).
[64] P. Su, Z. Tang, and W. Wu, WIREs Comput. Mol. Sci. **10**, e1460 (2020).
[65] J. X. Zou, *Molecular Orbital Kit (MOKIT)*, https://gitlab.com/jxzou/mokit, accessed May, (2025).
[66] M. E. Casida, J. Mol. Struct.: THEOCHEM **914**, 3 (2009).
[67] M. A. L. Marques, C. A. Ullrich, F. Nogueira, A. Rubio, K. Burke, and E. K. U. Gross, *Time-dependent Density Functional Theory*, Springer, Berlin, (2006).
[68] B. A. Hess, C. M. Marian, U. Wahlgren, and O. Gropen, Chem. Phys. Lett. **251**, 365 (1996).
[69] F. Neese, J. Chem. Phys. **122**, 034107 (2005).
[70] B. A. Hess, Phys. Rev. A **32**, 756 (1985).
[71] M. Douglas and N. M. Kroll, Ann. Phys. **82**, 89 (1974).
[72] B. A. Hess, Phys. Rev. A **33**, 3742 (1986).
[73] D. A. Pantazis, X. Y. Chen, C. R. Landis, and F. Neese, J. Chem. Theory Comput. **4**, 908 (2008).
[74] M. Buehl, C. Reimann, D. A. Pantazis, T. Bredow, and F. Neese, J. Chem. Theory Comput. **4**, 1449 (2008).
[75] D. A. Pantazis and F. Neese, J. Chem. Theory Comput. **7**, 677 (2011).
[76] D. A. Pantazis and F. Neese, Theor. Chem. Acc. **131**, 1292 (2012).
[77] J. D. Rolfes, F. Neese, and D. A. Pantazis, J. Comput. Chem. **41**, 1842 (2020).
[78] F. Neese, F. Wennmohs, A. Hansen, and U. Becker, Chem. Phys. **356**, 98 (2009).
[79] R. Izsak and F. Neese, J. Chem. Phys. **135**, 144105 (2011).
[80] F. Neese, WIREs Comput. Mol. Sci. **12**, e1606 (2022).

DOI: 10.1063/1674-0068/cjcp2505073